




Submitted: July 4, 2024

Revised: October 7, 2024

Accepted: October 21, 2024

# S-parameters of flexible electromagnetic radiation shields with Fe-Ni system coating

A.D. Gladinov , O.V. Boiprav , V.A. Bogush 

Belarusian State University of Informatics and Radioelectronics, Minsk, Belarus

 mr.gladinov@mail.ru

## ABSTRACT

The results of studies of 2.0–17.0 GHz frequency responses of  $S_{11}$  and  $S_{21}$  values of flexible electromagnetic radiation shields made of metallized polymer film, on the surface of which a coating of the Fe–Ni system is applied by electron beam evaporation, are presented. It has been experimentally established that an alloy in the Fe–Ni system containing 56 wt. % (~ 57 at. %) Fe and 44 wt. % (~ 43 at. %) Ni is azeotropic one. Such composition corresponds to the minimum temperature at which the total vapor pressure reaches 10 Pa. It has been determined that by applying of the Fe–Ni system coating with the specified content of components to the surface of a metallized polymer film, it is possible to reduce  $S_{11}$  value by a maximum of 5.0 dB and  $S_{21}$  value by a maximum of 6.7 dB in the frequency range of 2.0–17.0 GHz of this film.

## KEYWORDS

flexible shield • electromagnetic radiation • Fe–Ni system • electron beam evaporation

**Citation:** Gladinov AD, Boiprav OV, Bogush VA. S-parameters of flexible electromagnetic radiation shields with Fe-Ni system coating. *Materials Physics and Mechanics*. 2024;52(5): 74–82.

[http://dx.doi.org/10.18149/MPM.5252024\\_8](http://dx.doi.org/10.18149/MPM.5252024_8)

## Introduction

Electromagnetic radiation (EMR) shielding is currently a pressing chronic problem due to the continuous development of radio-electronic devices, especially with wireless power supplies, which has necessitated the constant improvement of means of protection against negative electromagnetic interference. In recent years, employees of Belarusian State University of Informatics and Radioelectronics, based on the results of their research, have developed various devices for EMR shielding.

Thus, at the research laboratory "Materials, Technologies and Equipment for Safety" of Belarusian State University of Informatics and Radioelectronics, the following main kinds of EMR shields have been developed:

1. non-flammable shields based on aluminum oxide and magnetic powder [1];
2. shields based on fabric materials [2,3].

One of the current directions of the research work conducted in the indicated laboratory is development of EMR shields based on foil and foiled film materials [4,5]. EMR shields based on foil, or foiled (metallized) film materials are also direction of the work conducted by the other researchers [6–10]. The main advantage of such materials is their thinness and flexibility. Due to this advantage it's possible to modify the shape of the shields based on these materials. Such materials are widely used nowadays for obtaining EMR shields with frequency selective surface (metasurface) [11–19]. Moreover, origami technic is widely used nowadays to create EMR shields based on such materials [20–29].

All of the above shields are composite structures that provide a high degree of EMR shielding. At the same time, the use of thin-film vacuum coatings for EMR shielding systems, combining metal layers with high values of electrical conductivity (Al, Cu) and relative magnetic permeability (Ni, Fe), is one of the little-studied and promising areas. The choice of the electron beam evaporation method for the Fe–Ni system films obtaining is primarily due to the impossibility of using magnetron sputtering methods due to the shielding of the magnetron cathode unit magnetic field by targets. Since electron beam evaporation causes alloy fractionation, the azeotropic composition of the alloy was calculated for the Fe–Ni system. The relevance of the work is due to the ever-increasing requirements for noise immunity of electronic devices.

This article discusses the results of studies of the protective properties of flexible EMR screens made of metallized polymer film with coatings of the Fe–Ni system formed on their surface by electron beam evaporation.

### Justification of the composition of Fe–Ni system coating

As follows from the phase diagram (Fig. 1), Fe–Ni system alloys are unlimited solid solutions, therefore, during their electron beam evaporation, the liquid → vapor phase transition obeys Raoult's law. The sizes of the elements radii near their melting temperatures,  $R_{Fe} = 0.1290$  nm,  $R_{Ni} = 0.1246$  nm. Therefore, Fe and Ni activities ratio in accordance with [30] is equal to:

$$\frac{f_{Fe}}{f_{Ni}} = \left(\frac{R_{Fe}}{R_{Ni}}\right)^3 = \left(\frac{0.1290}{0.1246}\right)^3 = 1.11. \quad (1)$$

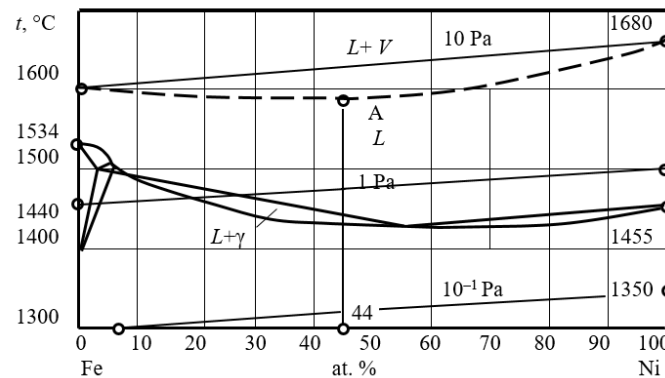


Fig. 1. State diagram of the Fe–Ni system (L – liquid; V – vapor;  $\gamma$  –  $\gamma$ -phase)

The required rate of deposition of Fe–Ni systems coatings with a thickness of 150 nm is ensured at a Ni and Fe vapor pressure ranging from 1 to 20 Pa. According to Fig. 1, the evaporation temperatures of Ni–Fe system alloys should be in the range from 1500 to 1650 °C. The average pressure of Fe vapor in this temperature range is 13 Pa, and that of Ni vapor is 11 Pa [30]. The atomic masses of the elements Ni and Fe are 58.71 and 55.85 amu. respectively.

Substituting all the indicated values into Eq. (1), for the Fe–Ni system we obtain:

$$\frac{n_{Ni}}{n_{Fe}} = \frac{f_{Ni}x_{Ni}P_{Ni}}{f_{Fe}x_{Fe}P_{Fe}} \left(\frac{A_{Fe}}{A_{Ni}}\right)^{1/2} \text{ at } \frac{n_{Ni}}{n_{Fe}} = 1, \text{ we get } x_{Fe} = 1.11 \cdot \left(\frac{13}{11}\right) \cdot \left(\frac{58.71}{55.85}\right)^{1/2} \cdot x_{Ni} = 1.345 \cdot x_{Ni}. \quad (2)$$

From equation  $x_{Fe} + x_{Ni} = 1$  we find that  $x_{Fe} = 0.574$ ;  $x_{Ni} = 0.426$ . Thus, according to the carried calculations out, it was established that Fe–Ni system alloy containing 56 wt. % (~57 at. %) Fe and 44 wt. % (~ 43 at. %) Ni is azeotropic one. Such composition corresponds to the minimum temperature value at which the total vapor pressure reaches 10 Pa (Fig. 1, point A on the isobar).

The reproducibility of the composition of layers of Ni–Fe system alloys obtained by electron beam evaporation was judged by the results of an analysis of their elemental composition. Nickel grade NP2 and iron 005ZhR were used as starting materials. Five samples of alloys were prepared from these materials. The compositions of the alloys, as well as the average content of elements in coatings 150 nm thick, are given in Table 1. Each value was obtained from elemental analysis data of at least 3 samples.

**Table 1.** Compositions of the Fe–Ni system alloys and average element contents in 150 nm thick coatings obtained by electron beam evaporation

| Alloy number | Alloy composition, at. % |    | 150 nm thick coatings composition, at. % |      |        |
|--------------|--------------------------|----|--|------|--------|
|              | Fe                       | Ni | Fe                                       | Ni   | Others |
| 1            | 30                       | 70 | 51.5                                     | 45.4 | 3.1    |
| 2            | 40                       | 60 | 38.8                                     | 58   | 3.2    |
| 3            | 55                       | 45 | 51                                       | 47.6 | 1.4    |
| 4            | 60                       | 40 | 58.7                                     | 38.8 | 2.5    |
| 5            | 70                       | 30 | 68.5                                     | 28.7 | 2.8    |

It can be seen that the elemental composition of the films is preserved upon evaporation of the  $Fe_{55}Ni_{45}$  alloy, i.e. its congruent evaporation occurs. At the same time, as follows from Table 1, due to the very similar values of vapor pressure, molecular weights, parameters of the crystal lattices of Fe and Ni, as well as the unlimited solubility of these elements in melts, the elemental composition of films of the Fe–Ni system is quite close to all the compositions of evaporated alloys that we have studied.

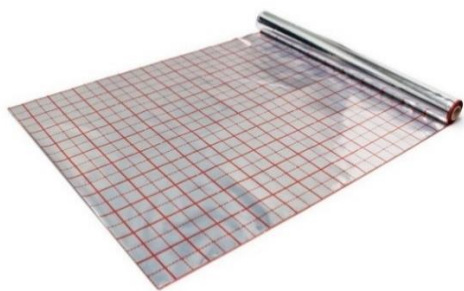


**Fig. 2.** The appearance of the film Kotar IZOFOLIX

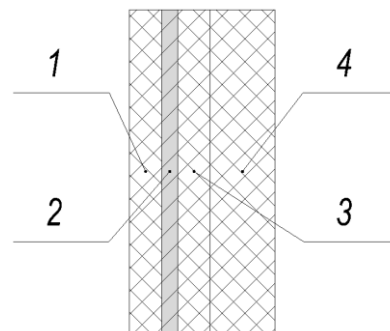


**Fig. 3.** Layers' layout of the film Kotar IZOFOLIX:

1, 3 – polypropylene film; 2 – aluminum layer; 4 – polyethylene layer

Kotar IZOFOLIX film was chosen as a polymer base for the coating [31]. This film has a thickness of 105  $\mu\text{m}$ . It has multilayer structure, one of the layers of which is aluminum with a thickness of 150 nm. The appearance of this film is shown in Fig. 2, and its layers' layout is shown in Fig. 3.

An alloy of composition  $\text{Fe}_{55}\text{Ni}_{45}$  was used as material for applying coatings by electron beam evaporation. Coatings were applied to the polymer substrate using a VU-1A installation according to the following regime:

1. the residual gas pressure in the chamber was no more than  $5 \cdot 10^{-2}$  Pa;
2. the substrate temperature was no more than 40 °C;
3. the application time was 150 s;
4. the application speed was 1 nm/s;
5. the distance from the crucible to the polymer substrate was 400 mm;
6. the weight of the sample was 20 g.

In this case, the thickness of the applied Fe–Ni system coating was 150 nm. The choice of this thickness value is due to the low heat resistance of the polymer substrate. At a coating application rate of 1 nm/s and a process duration of more than 150 s, the substrate is destroyed. The layers' layout of the EMR shield obtained according to the presented method is shown in Fig. 4.

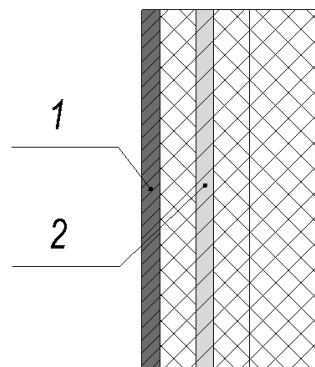


**Fig. 4.** Layers' layout of the EMR shield:  
1 – coating of the Fe–Ni system; 2 – the film Kotar IZOFOLIX

## Methods

The measurements of the EMR reflection and transmission coefficients the shields ( $S_{11}$  and  $S_{21}$  values, respectively) were carried out in the frequency range of 2.0–17 GHz. The panoramic meter of transmission and reflection coefficients SNA 0.01–18 was used for the measurements. The measurements were carried out in accordance with Standard 20271.1–91 "Microwave electronic products. Methods for measuring electrical parameters". The modulus of the measurements relative error of EMR reflection and transmission coefficients doesn't exceed 10.0 %. The connection diagrams of the modules of this meter are shown in Fig. 5.

The dimensions of the studied EMR shields samples were 300 × 400 mm. The following EMR shields samples were studied:

1. single-layer EMR shield sample based on Kotar IZOFOLIX film (Fig. 3), sample 1.1;
2. double-layer EMR shield sample based on Kotar IZOFOLIX film (Fig. 6), sample 1.2;
3. single-layer EMR shield sample based on Kotar IZOFOLIX film, on the surface of which a 150 nm coating from  $\text{Fe}_{55}\text{Ni}_{45}$  alloy was applied (Fig. 4), sample 2.1;

4. double-layer EMR shield sample based on Kotar IZOFOLIX film, on the surface of which 150 nm coating from Fe<sub>55</sub>Ni<sub>45</sub> alloy was applied (Figs. 7,8), samples 2.2 and 2.3, respectively.

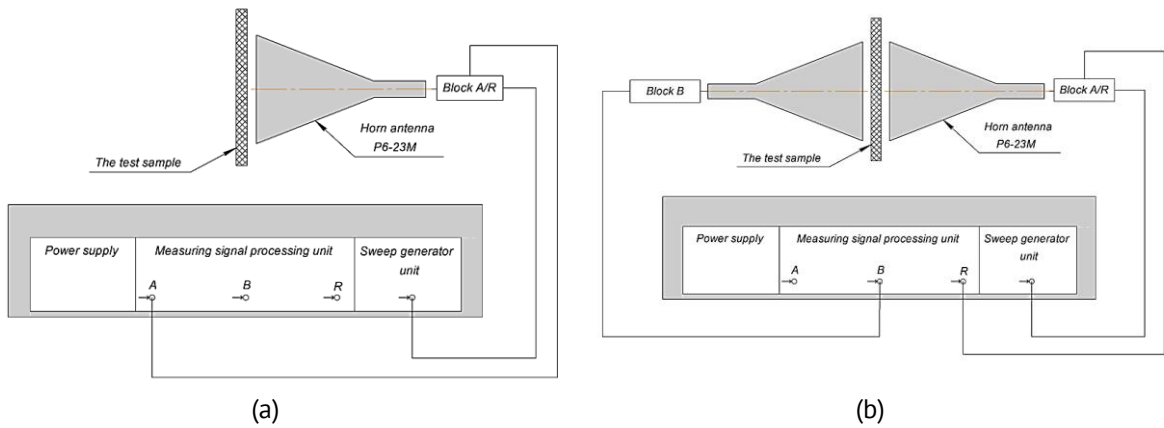


**Fig. 5.** The connection diagrams of the modules of panoramic meter of transmission and reflection coefficients SNA 0.01–18 for S11 value (a) and S21 value (b) measuring

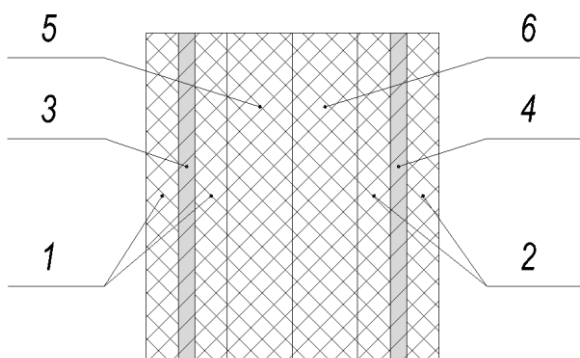


**Fig. 6.** Layers layout of the sample 1.2: 1, 2 – polypropylene film; 3, 4 – aluminum layer; 5, 6 – polyethylene layer

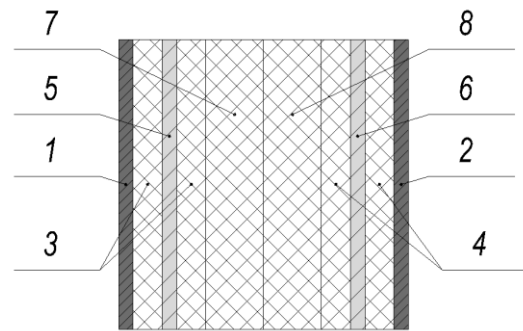


**Fig. 7.** Layers' layout of the sample 2.2: 1, 2 – coating of the Fe–Ni system; 3, 4 – polypropylene film; 5, 6 – aluminum layer; 7, 8 – polyethylene layer

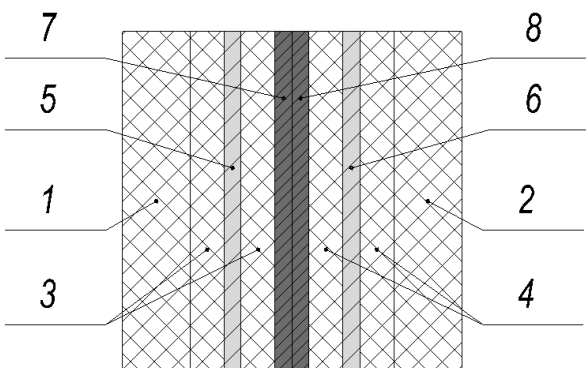


**Fig. 8.** Layers' layout of the sample 2.3: 1, 2 – polyethylene layer; 3, 4 – polypropylene film; 5, 6 – aluminum layer; 7, 8 – coating from Fe<sub>55</sub>Ni<sub>45</sub> alloy



**Fig. 9.** External view of the measuring unit IUS-3 with an installed sample

Measurement of the surface resistance of the sample 2.1 was performed. The measuring unit IUS-3 was used for this (Fig. 9).

The surface resistance ( $\rho_s$ ) of the indicated sample was measured using the four-probe method under the following conditions: the probes were arranged in a row at five points; the distance between the probes was 1 mm; slides measuring  $75 \times 25 \times 2 \text{ mm}^3$  were used as substrates.

Based on the results of such measurements, the specific surface resistance ( $\rho$ ) of the sample was calculated according to the following equation:

$$\rho = \rho_s \cdot t, \quad (3)$$

where  $t$  is the sample thickness.

## Results and Discussion

2–17 GHz frequency responses of  $S_{11}$  values of the samples 1.1 and 1.2 are presented on Fig. 10.

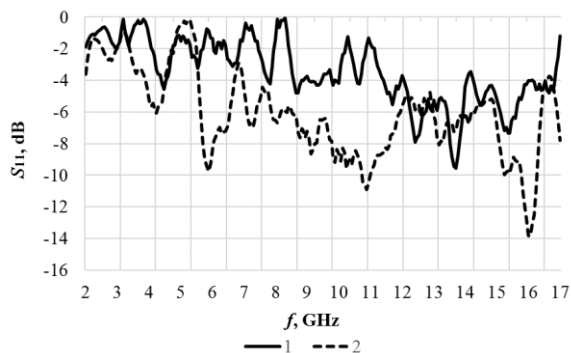


**Fig. 10.** 2–17 GHz frequency responses of  $S_{11}$  values of the samples 1.1 (curve 1) and 1.2 (curve 2)

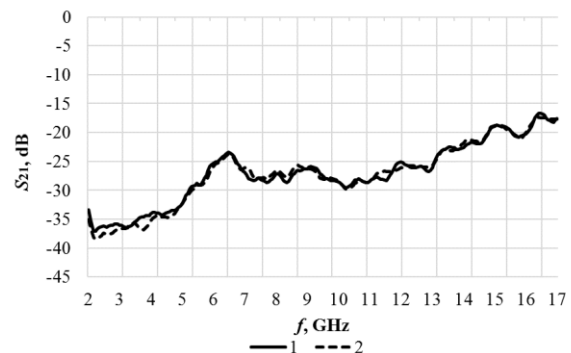


**Fig. 11.** 2–17 GHz frequency responses of  $S_{21}$  values of the samples 1.1 (curve 1) and 1.2 (curve 2)

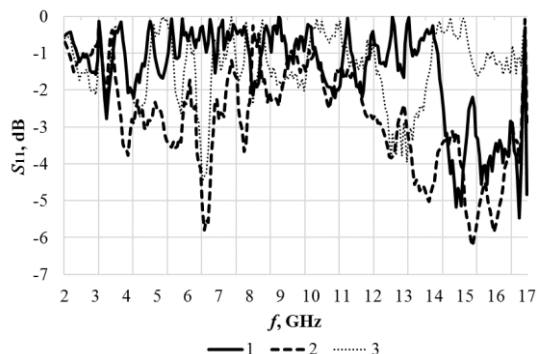


**Fig. 12.** 2–17 GHz frequency responses of  $S_{11}$  values of the samples 2.1 (curve 1), 2.2 (curve 2) and 2.3 (curve 3)

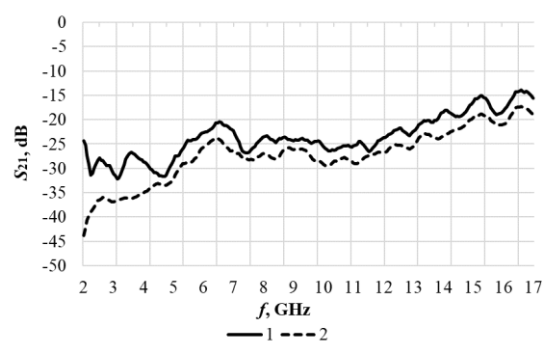


**Fig. 13.** 2–17 GHz frequency responses of  $S_{21}$  values of the samples 2.1 (curve 1), 2.2 and 2.3 (curve 2)

In the frequency range 2–17 GHz,  $S_{11}$  values change from -9.4 to -0.04 dB and from -13.8 to -0.14 dB for the samples 1.1 and 1.2 respectively. It should be noted that when the number of layers in the shield based on the film Kotar IZOFOLIX increases from one to two, the energy of the EMR reflected from it decreases. This phenomenon is most clearly observed in the frequency ranges of 5–7, 10–12 and 15–16 GHz. This



phenomenon is associated with the resonant interaction in antiphase of the EMR of the listed frequency ranges. 2–17 GHz frequency responses of S21 values of the samples 1.1 and 1.2 are presented on Fig. 11.

In the frequency range of 2–17 GHz, S21 values change from -36.5 to -16.6 dB and from -38.2 to -17.4 dB for of the samples 1.1 and 1.2 respectively. Thus, increasing the number of layers in shields based on film Kotar IZOFOLIX doesn't have a significant effect on their S21 values. 2–17 GHz frequency responses of S11 values of the samples 2.1, 2.2 and 2.3 are presented on Fig. 12.

In the frequency range of 2–17 GHz, S11 values vary from -5.5 to -0.017 dB for the sample 2.1, from -6.2 to -0.25 dB for the sample 2.2, and from -4.4 to -0.006 dB for the sample 2.3. 2–17 GHz frequency response of S11 value of the sample 2.2 is characterized by a resonant decrease in the frequency ranges of 5–7 and 14–16 GHz. 2–17 GHz frequency responses of S21 values of the samples 2.1, 2.2 and 2.3 are presented on Fig. 13.

S21 values vary from -33.0 to -14.2 dB for the sample 2.1 and 2.2 and from -43.7 to -17.3 dB for the samples 2.3. Thus, an increase from one to two layers in the shield based on film Kotar IZOFOLIX, on the surface of which a 150 nm coating of Fe<sub>55</sub>Ni<sub>45</sub> alloy is applied, leads to a decrease by 3–18 dB in the S21 value of this shield.

The relative measurement error of the surface resistance of coatings using the four-probe method doesn't exceed 5.0 %. To reduce the measurement error, the results of five measurements of the specified parameter for each sample were averaged.

The results of surface resistance measurements of the sample 2.1 are presented in Table 2.

**Table 2.** The results of surface resistance measurements of the sample 2.1

| Area No. 1,<br>Ω/ square | Area No. 2,<br>Ω/ square | Area No. 3,<br>Ω/ square | Area No. 4,<br>Ω/ square | Area No. 5,<br>Ω/ square |
|--------------------------|--------------------------|--------------------------|--------------------------|--------------------------|
| 39.3                     | 47.9                     | 42.3                     | 53.1                     | 58.8                     |

Based on the results of calculations carried out using Eq. (3), it was determined that the specific surface resistance of a 150 nm coating of Fe<sub>55</sub>Ni<sub>45</sub> alloy is  $7.242 \cdot 10^{-6} \Omega \cdot \text{m}$ :  $\left(\frac{39.3+47.9+42.3+53.1+58.8}{5}\right) \cdot 150 \cdot 10^{-9} = 48.28 \Omega/\text{square} \cdot 150 \cdot 10^{-9} \text{ m} = 7.242 \cdot 10^{-6} \Omega \cdot \text{m}$ .

## Conclusions

Calculations of the parameters of the compositions a coating of Fe–Ni alloys were carried out. Based on the results of such calculations, it was found that the Fe<sub>55</sub>Ni<sub>45</sub> alloy is azeotropic one. The mode of applying a 150 nm coating of this alloy onto a substrate in the form of a foil-clad polypropylene film (film Kotar IZOFOLIX) was developed.

It was found that applying a 150 nm coatings of Fe<sub>55</sub>Ni<sub>45</sub> alloy onto film Kotar IZOFOLIX allows to reduce its S11 value by a maximum of 5 dB, and S21 value by a maximum of 6.7 dB. When increasing the number of layers in the shield based on film Kotar IZOFOLIX from one to two, its S11 value decreases by a maximum of 10 dB. S21 value remains virtually unchanged. Increasing the number of layers in the shield based on film Kotar IZOFOLIX, on the surface of which a 150 nm coating of Fe<sub>55</sub>Ni<sub>45</sub> alloy

is applied, from one to two leads to a decrease by a maximum of 5 dB in the S11 value of such shield. It's S21 value decreases by 3–18 dB in such case. It was determined that the specific surface resistance of a 150 nm coating of Fe<sub>55</sub>Ni<sub>45</sub> alloy is  $7.242 \times 10^{-6} \Omega \cdot \text{m}$ .

## References

1. Penialosa Ovalies DI, Boprav OV, Tumilovich MV, Lynkou LM. Electromagnetic Radiation Shielding Composite Coatings Based on Powdered Alumina and Iron Oxides. *Doklady BGUIR*. 2021;19(3): 104–109.
2. Boprav OV, Ahmed AAA, Lynkou LM. Electromagnetic Radiation Reflection and Transmission Characteristics of Shielding Polyester Fabric with Nanostructured Ferromagnetic Microwire, Containing Copper Clusters. *Doklady BGUIR*. 2015;3(89): 49–52. (In Russian)
3. Abdulhadi HA, Almashat EA, Boprav OV, Bogush VA, Prudnik AM. Electromagnetic and Sound Insulation Properties of Combined Shields Based on the Needle-Punching Material and Fragments of Aluminum Foil. *Doklady BGUIR*. 2020;18(1): 89–95. (In Russian)
4. Boprav OV, Lynkou LM, Mukhurov NI, Al-Mashat EAA. Electromagnetic Radiation Shields Based on Anodic Aluminum Oxide. *Doklady BSUIR*. 2018;7(117): 159–161.
5. Boprav O, Hasanov M, Bogush V, Lynkou L. Flexible Double-Layered Microwave Absorbers Based on Foiled Materials with Mechanically Treated Surface. *New Materials, Compounds and Applications*. 2023;7(2): 100–110.
6. Rambung E, Kalanjati VP, Abdurachman. Aluminum Foil Shield Diminishes the Electromagnetic Radiation of Mobile Phones in the Cerebellum of Adult Male Rats. In: *Proceedings of Surabaya International Physiology Seminar (SIPS 2017)*. 2017: 97–100.
7. Li W, Jin H, Zeng Z, Zhang L, Zhang H, Zhang Z. Flexible and easy-to-tune broadband electromagnetic wave absorber based on carbon resistive film sandwiched by silicon rubber/multi-walled carbon nanotube composites. *Carbon*. 2017;121: 544–551.
8. Kim T, Wan Do H, Choi KJ, Kim S, Lee M, Kim T, Yu BK, Cheon J, Min BW, Shim W. Layered Aluminum for Electromagnetic Wave Absorber with Near-Zero Reflection. *Nano Letters*. 2021; 21(2): 1132–1140.
9. Hwang U, Kim J, Seol M, Lee B, Park IK, Suhr J, Nam JD. Quantitative Interpretation of Electromagnetic Interference Shielding Efficiency: Is It Really a Wave Absorber or a Reflector? *ACS Omega*. 2022;7(5): 4135–4139.
10. Lu Z, Zhang Y, Wang H, Xia C, Liu Y, Dou S, Li Y, Tan J. Transparent Thermally Tunable Microwave Absorber Prototype Based on Patterned VO<sub>2</sub> Film. *Engineering*. 2023;29: 198–206.
11. Hussein MN, Zhou J, Huang Y, Kod M, Sohrab AP. A Miniaturized Low-Profile Multilayer Frequency-Selective Surface Insensitive to Surrounding Dielectric Materials. *IEEE Transactions on Microwave Theory and Techniques*. 2017;65(12): 4851–4860.
12. Zhou Z, Chen K, Zhao J, Chen P, Jiang T, Zhu B, Feng Y, Li Y. Metasurface Salisbury screen: achieving ultra-wideband microwave absorption. *Optics Express*. 2017;24(24): 30241–30252.
13. Wang P, Zhang Y, Chen H, Zhou Y, Jin F, Fan H. Broadband radar absorption and mechanical behaviors of bendable over-expanded honeycomb panels. *Composites Science and Technology*. 2018;162: 33–48.
14. Chakradhary VK, Baskey HB, Roshan R, Pathik A, Akhtar MJ. Design of Frequency Selective Surface-Based Hybrid Nanocomposite Absorber for Stealth Applications. *IEEE Transactions on Microwave Theory and Techniques*. 2018;66(11): 4737–4744.
15. Xu Y, He M. Design of Multilayer Frequency-Selective Surfaces by Equivalent Circuit Method and Basic Building Blocks. *International Journal of Antennas and Propagation*. 2019: 9582564.
16. Dutta R, Mitra D, Ghosh J. Dual-band multifunctional metasurface for absorption and polarization conversion. *International Journal of RF and Microwave Computer-Aided Engineering*. 2020;30: e22200.
17. Qian J, Gou P, Pan H, Zhu L, Gui YS, Hu CM, An Z. Hybrid Perfect Metamaterial Absorber for Microwave Spin Rectification Applications. *Scientific Reports*. 2020;10: 19240.
18. Zhang Z, Zhao Y, Fan G, Zhang W, Liu Y, Liu J, Fan R. Paper-Based Flexible Metamaterial for Microwave Applications. *EPJ Applied Metamaterials*. 2021;8: 6.
19. Shen Y, Pang Y, Wang J, Ma H, Pei Z, Qu S. Origami-inspired metamaterial absorbers for improving the larger-incident angle absorption. *Journal of Physics D: Applied Physics*. 2015;48(44): 445008.
20. Zhang J, Liu S, Zhang L, Wang C. Origami-Based Metasurfaces: Design and Radar Cross Section Reduction. *AIAA Journal*. 2020;58(12): 5478–5482.



21. Chen X, Li W, Wu Z, Zhang Z, Zou Y. Origami-based microwave absorber with a reconfigurable bandwidth. *Optics Letters*. 2021;46(6): 1349–1352.
22. Fan X, Pan Z, Chen S, Li Y, Zhao Z, Xin Y, Pan T. Design and fabrication of a reconfigurable and flexible frequency selective surface with a buckling dipole via mechanical stretching. *Soft Science*. 2021;1(13).
23. Biswas A, Zekios CL, Ynchausti C, Howell LL, Magleby SP, Georgakopoulos SV. An ultra-wideband origami microwave absorber. *Scientific Reports*. 2022;12(1): 13449.
24. Zhu Z, Wang H, Li Y, Meng Y, Wang W, Zheng L, Wang J, Zhang J, Qu S. Origami-Based Metamaterials for Dynamic Control of Wide-Angle Absorption in a Reconfigurable Manner. *IEEE Transactions on Antennas and Propagation*. 2022;70(6): 4558–4568.
25. Yao J, Gui D, Zhang D, Zhang H. Ultra-Broadband Origami Absorber with Large Angle Stability in the THz Region. *Journal of the Optical Society of America B*. 2022; 39(10); 2603–2609.
26. Sun Y, Gao C, Chen L, Han L. A Design Method for Rectangular Waveguide-Typed Microwave Devices Based on a Novel Origami Process. *Materials*. 2023;16(24): 7625.
27. Zhang Z, Lei H, Duan S, Zhao Z, Chen M, Wang C, Fang D. Bioinspired Double-Broadband Switchable Microwave Absorbing Grid Structures with Inflatable Kresling Origami Actuators. *Advanced Science*. 2024;11(4): 2306119.
28. Song Z, Zhu JF, Wang X, Zhang R, Min P, Cao W, He Y, Han J, Wang T, Zhu J, Wu L, Qiu CW. Origami metamaterials for ultra-wideband and large-depth reflection modulation. *Nature Communications*. 2024;15: 3181.
29. Zhu Z, Li Y, Qin Z, Jiang L, Wang W, Chen H, Wang J, Zheng L, Qu S. Miura-Ori Based Reconfigurable Multilayer Absorber for High-Efficiency Wide-Angle Absorption. *Optics Express*. 2024;32(14): 24091–24106.
30. Zelenin VA, Narushko EO, Gladinov AD. Formation of Films of Alloys of Cr–Ni, Cr–Ni–Si and Fe–Ni Systems by Sublimation and Evaporation Methods for Electronic Products. *Doklady BGUIR*. 2023;21(5): 5–12. (In Russian)
31. *Insulating foil IZOFOLIX*. URL: <https://www.kotar.pl/ru/oferta/folie-izolacyjne/108-folia-izolacyjna-izofolix-rus> (In Russian)

## About Authors

**Anton D. Gladinov** 

*Junior Researcher (Belarusian State University of Informatics and Radioelectronics, Minsk, Belarus)*

**Olga V. Boiprav**  

*Candidate of Technical Sciences*

*Associate Professor (Belarusian State University of Informatics and Radioelectronics, Minsk, Belarus)*

**Vadim A. Bogush**  

*Doctor of Physical and Mathematical Sciences*

*Rector (Belarusian State University of Informatics and Radioelectronics, Minsk, Belarus)*